

## Article

# Effects of Non-Thermal Plasma on the Transition from Nano-Crystalline to Amorphous Structure in Water and Subsequent Effects on Viscosity

Joshua Ginzburg<sup>1</sup>, Mobish Shaji<sup>1,\*</sup> , Alexander Rabinovich<sup>1</sup>, Dmitri Vainchtein<sup>1</sup>, Christopher Sales<sup>2</sup>  and Alexander Fridman<sup>1</sup>

<sup>1</sup> C and J Nyheim Plasma Institute, Drexel University, Camden, NJ 08103, USA

<sup>2</sup> Department of Civil, Architectural and Environmental Engineering, Drexel University, Philadelphia, PA 19104, USA

\* Correspondence: ma3748@drexel.edu

**Abstract:** Recent studies have demonstrated that the physical properties of water treated with non-thermal plasma, or plasma-activated water (PAW), significantly differ from those of distilled water. For example, contrary to expectation, the viscosity of PAW becomes lower than that of distilled water at certain temperatures. This study developed a model to explain these differences by combining the two-state model of ordinary water, which describes water as a combination of nano-crystalline clusters and amorphous, free-floating molecules, using the Debye–Huckel theory for a fluid containing ions. A model for the viscosity of PAW was then developed from the general model. It explains how PAW has a lower viscosity than distilled water as the temperature decreases and why this effect is stronger than the colligative effect for ideal solutions. Finally, the viscosity model is compared to the experimental measurements of PAW treated with gliding arc plasma, showing that the data match the predicted values quite well. The model of PAW developed here can be used to understand other physical properties beyond viscosity, such as the surface tension, contact angle, electric conductivity, heat capacity, isothermal compressibility, and density, potentially facilitating new applications of PAW.

**Keywords:** plasma-activated water (PAW); physical properties of PAW; viscosity of PAW; crystalline structure in PAW; amorphous structure in PAW; viscosity model of PAW



**Citation:** Ginzburg, J.; Shaji, M.; Rabinovich, A.; Vainchtein, D.; Sales, C.; Fridman, A. Effects of Non-Thermal Plasma on the Transition from Nano-Crystalline to Amorphous Structure in Water and Subsequent Effects on Viscosity. *Plasma* **2024**, *7*, 16–28. <https://doi.org/10.3390/plasma7010002>

Academic Editors: Tariq Rafiq and Andrey Starikovskiy

Received: 10 December 2023

Accepted: 15 December 2023

Published: 21 December 2023



**Copyright:** © 2023 by the authors. Licensee MDPI, Basel, Switzerland. This article is an open access article distributed under the terms and conditions of the Creative Commons Attribution (CC BY) license (<https://creativecommons.org/licenses/by/4.0/>).

## 1. Introduction

Plasma is the fourth state of matter in which a certain portion of particles in a gas or liquid are ionized. The ionization of neutral particles is often achieved by heating; as the temperature increases, the molecules become more energetic and transform from solid to liquid, from liquid to gas, and finally, from gas to plasma state. The major features of plasma are high temperatures exceeding conventional sources, the ability to produce very high concentrations of energetic and chemically active species (e.g., electrons, ions, atoms, and radicals in excited states), and the ability to be essentially far from thermodynamic equilibrium, thereby providing very high concentrations of chemically active species while keeping the bulk temperature as low as room temperature [1].

In gases, the temperature of plasma is determined by the average energies of its particles (neutral and charged) and their degrees of freedom (translational, rotational, vibrational, and those related to electronic excitation). Since plasma systems are multi-component systems, they are able to exhibit multiple temperatures. During the electric discharges that generate plasma, electrons receive energy from an electric field during their mean free path. The subsequent collisions of electrons with heavy particles can equilibrate their temperatures; quasi-equilibrium plasma of this kind is called thermal plasma. But

if the time or energy are not sufficient, an equilibration of temperatures will not occur; non-equilibrium plasma of this kind is called non-thermal plasma [1].

The non-equilibrium nature of non-thermal plasma can produce very high concentrations of chemically active species while keeping bulk temperatures as low as room temperature. These characteristics aid its use in material processing, for pollutant treatments, in biomedical applications, medicine, space craft sterilization, hydrogen sulfide mitigation, PFAS mitigation, agricultural applications, and beyond [2–17].

When water is treated with non-thermal plasma, reactive oxygen and nitrogen species are transferred to water, leading to the formation of secondary active species such as OH radicals, ozone, hydrogen peroxide, nitrites, nitrates, peroxyxynitrites, and peroxyxynitrates [2]. The addition of these species gives plasma-activated water (PAW) many potential applications as an eco-friendly alternative in disinfection and seed germination; as a fertilizer and insecticide; in curing plant infections; preserving produce; wound healing; the deactivation of bacteria, viruses, and fungi; and the selective killing of cancer cells [18–24]. While the chemical properties and capabilities of PAW have been extensively researched, there have been far fewer studies of the physical effects of plasma activation on water.

A recent study by J He et al. [25] found that when used to eliminate *E. coli* from fresh produce, PAW was not only able to chemically inactivate the *E. coli*, but it also showed an improved washing-out capability compared to water, meaning that PAW had a more effective physical ability to clear out *E. coli* located inside microscopic pores in the produce surface. This indicates that PAW has a lower surface tension than normal water. Such a finding gives PAW a wide new range of possible applications as a surfactant. Until the study by Shaji et al. [26] on the physical properties of PAW, the investigated physicochemical properties of PAW included only pH, ORP, and electrical conductivity; these properties were investigated in relation to the chemical properties and behavior of PAW, as they are indicators of reactive species in the PAW [26].

The study by M Shaji et al. [26] showed that other physical properties of water such as the viscosity and contact angle are also affected by plasma activation, as is surface tension. Plasma activation results in a lower surface tension, lower contact angles on glass surfaces, lower viscosities at low temperatures, and higher viscosities at high temperatures relative to water. The authors reported that plasma addition leads to the lowering of the mesoscopic transition temperature in water, resulting in water achieving an amorphous structural state at lower temperatures. The amorphous state is characterized by fewer hydrogen bonds between water molecules, which results in lower surface tension and viscosity compared to the crystalline structure, where water molecules are highly hydrogen-bonded to one another. Therefore, PAW at low temperatures has a lower surface tension and viscosity than water. As the temperature increases, the natural viscosity increasing effect of plasma species, which are larger than water molecules, will lead to an increase in the PAW viscosity relative to water. The lower contact angle in PAW was attributed to the plasma addition increasing the surface energy during contact between water and the surface of measurement (glass) [26]. It is quite surprising that the viscosity of PAW at low temperatures was shown to be lower than that of distilled water. It would be typically expected that the viscosity of a fluid would be increased by the addition of species which are larger than the fluid molecules and prevent the fluid from flowing as easily. Yet, the exact opposite effect was observed below roughly 15 °C. This behavior is similar to the effect salts have on low-temperature water.

The low surface tension of PAW signals the potential surfactant behavior of this liquid. Surfactants find use in many industrial processes, such as paints, food emulsions, biotechnological processes, biosciences, pharmaceuticals, and cosmetic products. PAW can find use as an eco-friendly and cost-effective alternative to the current products used for these applications. Since PAW is antibacterial, antifungal, and has the demonstrated ability to disinfect bacteria from fresh produce, it can also be used as a washing-out agent. Anti-bacterial and anti-fungal surfactants are presently used in the biomedical industry, so with these characteristics, PAW can be applied as a biomedical industrial surfactant.

Surfactants are also used in the production of detergents; PAW can be used as an eco-friendly ingredient in these processes. The major advantage of PAW is its biodegradability, allowing it to be used as an ingredient in many industrial processes without harming the environment [26].

The viscosity of PAW is influenced by mesoscopic structural changes and the presence of foreign plasma additives due to plasma activation. The mesoscopic structural changes due to foreign plasma additives from plasma activation result in changes in the viscosity behavior of PAW. At low temperatures, when the effect of the crystalline structure in pure water is strong, PAW, which has a more amorphous structure, has a slightly lower viscosity. When temperatures rise beyond low values, the friction-inducing plasma additives that are present in PAW will lead to a higher viscosity compared to water. Until water transitions from a crystalline structure to an amorphous structure, the viscosity of PAW will be only nominally higher than the viscosity of water. However, if the temperature increases beyond the mesoscopic transition temperature in water, it will attain an amorphous structure, and friction-causing plasma additives will lead PAW to have a significantly higher viscosity relative to water at these higher temperatures. The high viscosity of PAW can lead to it developing a higher shear force during its flow at high temperatures. The higher shear force exerted by the flow of PAW on a particle in its path can lead to a more efficient removal of particles when compared to normal water, resulting in PAW being a better cleaning agent at higher temperatures. The higher viscosity of PAW can also help it to develop a thicker boundary layer during flow, thereby reducing transfer losses and making it suitable for augmented oil extraction [26].

With respect to the contact angle, the addition of plasma results in water forming smaller contact angles on a glass surface, indicating that the addition of plasma increases the surface energy during the interaction between water and a glass surface. The addition of plasma also results in increased wettability and the increased adhesion of water droplets to a glass surface. Increased wettability and adhesion are of great use for applications in the surface treatment industry. These improved surface properties exhibited by PAW suggest that the plasma activation of liquids could result in improved adhesion and wettability characteristics in them, potentially improving the adhesive behaviors of paints, dyes, etc. [26]. PAW needs to be analyzed for these different applications to understand its applicability.

The noticeable and unusual effects on these properties indicate that PAW undergoes a significant structural change, which, if understood and modeled, could provide a method to understand PAW's unexpected influence on properties like viscosity. The aim of this study is to develop a model for this structural change and use this model to understand the viscosity of PAW's behavior.

## 2. Materials and Methods

### 2.1. Two-State Model of Liquid Water and the Effects of Plasma Activation

Due to their highly polar nature, water molecules have the tendency to create hydrogen bonds between one another even before their freezing point [27]. As a result, liquid water can exist in two possible structures: the amorphous state, where water molecules move freely and are not bonded to one another, and the nano-crystalline or structured state, where molecules begin to form bonds between one another, causing significant differences in density, surface tension, viscosity, and other physical properties. This tendency to begin forming structures significantly above the freezing temperature is the essence of water's unique and anomalous behavior compared to other liquids. The lower the temperature the water is brought to, the higher the proportion of nano-crystalline structures. Figure 1 shows a depiction of nano-crystalline and amorphous structures in water, as reported by Semak et al. [28]

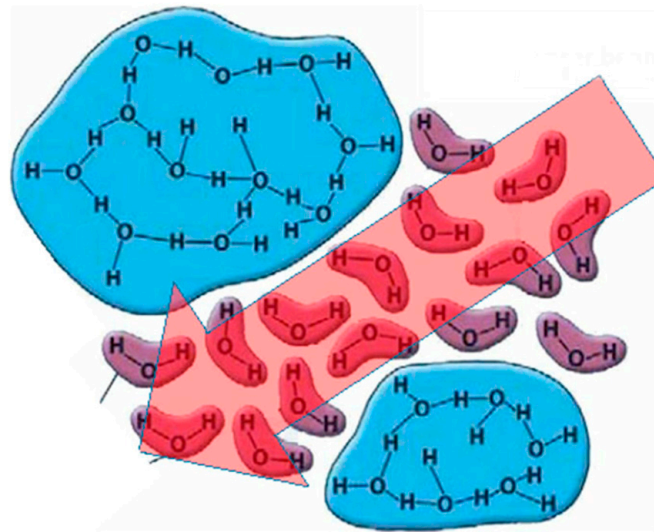


**Figure 1.** The two states of water, nano-crystalline in blue, and amorphous in red, adapted with permission from [28].

Although the transition between the amorphous and structured states involves a change of structure, it does not appear to be a first-order phase transition. A first-order transition would require the first derivative of free energy with respect to temperature to be discontinuous [29]. Entropy is given by  $s = -\frac{\delta f}{\delta T}$  [29]. Therefore, a first-order transition must have a discontinuous entropy, or in other words, a latent heat. This does not occur because the amorphous-to-structured transition happens gradually over a wide range of temperatures [30]. Since this is not a first-order transition, it can be classified as a continuous transition [31]. Further classifying the amorphous-to-nano-crystalline transition proves to be difficult. Many continuous transitions show a discontinuous second derivative of free energy with respect to temperature [32]. Isobaric heat capacity is given by  $C_p = T\left(\frac{\delta s}{\delta T}\right)_p$  [29], so a discontinuous second derivative of free energy with respect to temperature would result in a discontinuous  $C_p$ . However, while the amorphous to nano-crystalline transition is occurring, isobaric heat capacity remains continuous [30]. This is not even a general order–disorder transition since such a transition requires the formation of long range ordering, which is not always present in the nano-crystalline state [30,33]. As such, the given transition can best be described simply as a continuous short-range ordering transition.

As mentioned previously, when water is treated with non-thermal plasma, reactive oxygen and nitrogen species are transferred to the water, which, in turn, lead to the formation of secondary active species [2]. In effect, plasma activation causes the addition of ions to water, which can affect the amorphous-to-nano-crystalline transition. The presence of ions interferes with hydrogen bonding because the polar ends of water molecules that would otherwise be bonding to one another instead bond to ions. This behavior is identical to the ability of salts to lower the freezing temperature of water by interacting with hydrogen bonds [34]. This is why at lower temperatures, when there are more nano-crystalline structures present, PAW has the unexpected effect of lowering viscosity because the plasma species dissolve nano-crystalline structures and make it easier for the water to flow. Therefore, the plasma activation of water decreases the proportion of the structured state, particularly at low temperatures, and consequently causes changes in associated physical properties such as surface tension, viscosity, and contact angle [26].

## 2.2. Describing Pure Water with the Two-State Model

H. Tanaka [30] develops a model of ordinary liquid water and its anomalous behavior by considering its two possible structures. An equation is introduced for the Gibbs free

energy of water. Gibbs free energy is typically given by  $f = u + Pv - T\sigma$  [29], where  $f$  is Gibbs free energy,  $P$  is pressure,  $T$  is temperature, and  $u$ ,  $v$ , and  $\sigma$  are internal energy, volume, and entropy per unit structure, respectively. This equation was expanded by Tanaka et al. to account for the two different states of liquid water, which are structured and amorphous [30]:

$$f = [Su_s + (1 - S)u_a] + P[ Sv_s + (1 - S)v_a] + Tk_B \left[ S \ln \left( \frac{S}{g_s} \right) + (1 - S) \ln \left( \frac{1 - S}{g_a} \right) \right] \quad (1)$$

In the above Equation (1),  $S$  represents the bond order parameter, or the proportion of unit structures of the nano-crystalline state compared to the total number of unit structures,  $g$  is statistical degeneracy, and the subscripts  $s$  and  $a$  refer to the structured and amorphous states, respectively. The most likely candidate for the unit structure of the nano-crystalline state is the octameric unit of hexagonal ice [30]. Because the structured state has increased volume due to intermolecular repulsions in the nano-crystalline structures and far fewer degrees of freedom,  $u_a > u_s$ ,  $v_a < v_s$ , and  $g_a \gg g_s$ .

For any thermodynamic system, equilibrium occurs when  $(df)_{T,P} = 0$  [29]. So, in this case, the equilibrium condition is  $\frac{\partial f}{\partial S} = 0$ . This yields

$$\frac{S}{1 - S} = \frac{g_s}{g_a} \exp \left[ \frac{(u_a - u_s) - P(v_s - v_a)}{k_B T} \right] = \frac{g_s}{g_a} \exp \left[ \frac{\Delta u - P\Delta v}{k_B T} \right] \quad (2)$$

Since  $g_a \gg g_s$ , if the temperature is not exceedingly low (which it cannot be in the liquid phase),  $\frac{S}{1 - S}$  will be quite small, meaning that the approximation  $\frac{S}{1 - S} \approx S$  can be made [32]. Therefore, Equation (2) becomes

$$S = \frac{g_s}{g_a} \exp \left[ \frac{\Delta u - P\Delta v}{k_B T} \right] \quad (3)$$

Tanaka then introduces models for the density, isothermal compressibility, heat capacity at constant pressure, and viscosity of water using the two-state model [30]. By fitting these models to experimental values, it is determined that  $\Delta u = 3.6$  kcal/mol,  $\Delta v = 9.98$  cm<sup>3</sup>/mol, and  $\frac{g_s}{g_a} = 8.1 \times 10^{-5}$ . Substituting these values into Equation (3) gives

$$S = 8.1 \times 10^{-5} \exp \left[ \frac{3.6 \frac{\text{kcal}}{\text{mol}} - P \times \frac{9.98 \text{cm}^3}{\text{mol}}}{k_B T} \right] = 8.1 \times 10^{-5} \exp \left[ \frac{14,900 \text{J} - P \times 1.01 \text{J/atm}}{8.31 \text{J/KT}} \right] \quad (4)$$

The model developed for viscosity, which is of particular interest to this study, uses the general viscosity formula,  $\eta = \eta_0 T^{3/2} \exp[E_a / (k_B T)]$ , where  $\eta$  is dynamic viscosity,  $\eta_0$  is a constant,  $T$  is temperature,  $k_B$  is Boltzmann's constant, and  $E_a$  is the activation energy required for viscous flow.  $E_a$  is predicted to be of the form  $E_a = E_a^B + \Delta E_a S$ , where  $E_a^B$  is the background activation energy, which would be the activation energy if the water in question were entirely amorphous, and  $\Delta E_a$  is the additional activation energy needed for water molecules in the structured state [29]. We now move on to develop similar models for PAW, accounting for the addition of active species.

### 2.3. Describing PAW with the Two-State Model

Plasma activation introduces charged species and non-charged active species into water. The charged species include species directly related to plasma interaction with water (for example, solvated electrons) and those charged species formed indirectly due to plasma interaction with water (for example,  $H^+$ ,  $NO_2^-$ , and  $NO_3^-$ ). In order to account for the effects of these charged species, a Debye-Huckel term, ' $U_{DH}$ ' [25], is introduced to the free energy relationship of water, as shown in Equation (5). To account for the effect

of non-charged plasma active species (for example:  $H_2O_2$ ,  $O_3$ ), a dimensionless term, ' $\mu'$ ', with a value close to 1 is used in the Debye–Huckel relationship, as seen in Equation (5):

$$U_{DH} = -\sum_{i=1}^M \frac{N_i z_i^2}{2} \frac{e^2 \kappa}{4\pi\epsilon_r \epsilon_0} \frac{1}{1 + \kappa a_i}, \quad \kappa^2 = \frac{2e^2}{\epsilon_r \epsilon_0 k_B T} \sum_{i=1}^M z_i^2 \mu n_i \quad (5)$$

Here, the subscript  $i$  indicates the type of ion species,  $N_i$  is the ion concentration,  $z_i$  is the ion charge,  $M$  is the number of ion species present,  $e$  is the charge of an electron,  $\epsilon_r$  is the dielectric permittivity of the medium,  $\epsilon_0$  is the dielectric permittivity of a vacuum,  $a_i$  is the ion radius, and  $\kappa$  is the inverse of the Debye screening length. The Debye–Huckel theory has several limitations which make it increasingly inaccurate for higher ion concentrations, higher ion charges, and ions, which are non-spherical [34]. However, it is a useful and simple approximation which provides excellent predictions at lower concentrations and charges.

The ions are most typically found outside of nano-crystalline structures since they are unlikely to penetrate hydrogen-bonded clusters, so their effects on free energy can be approximated to be proportional to the fraction of water in the amorphous state ( $1 - S_p$ ) [25]. Hence, the Gibbs free energy of PAW ( $f_p$ ), Equation (1), becomes

$$f_p = [S_p u_s + (1 - S_p) u_a] + P [S_p v_s + (1 - S_p) v_a] + T k_B \left[ S_p \ln \left( \frac{S_p}{g_s} \right) + (1 - S_p) \ln \left( \frac{1 - S_p}{g_a} \right) \right] + (1 - S_p) U_{DH} \quad (6)$$

where  $S_p$  represents the bond order parameter of PAW, and the definition of remaining terms in the above free energy shown in Equation (6) are the same as those defined for Equation (1). As before, equilibrium occurs when  $\frac{\partial f_p}{\partial S_p} = 0$  [29], in this case, yielding

$$\begin{aligned} \frac{S_p}{1 - S_p} &= \frac{g_s}{g_a} \exp \left[ \frac{(u_a - u_s) - P(v_s - v_a) + U_{DH}}{k_B T} \right] = \frac{g_s}{g_a} \exp \left[ \frac{\Delta u - P\Delta v + U_{DH}}{k_B T} \right] \\ &= 8.1 \times 10^{-5} \exp \left[ \frac{3.6 \text{ kcal/mol} - P \times 9.98 \text{ cm}^3/\text{mol} + U_{DH}}{k_B T} \right] \end{aligned} \quad (7)$$

Under typical conditions,  $U_{DH}$  is expected to be roughly at the order of  $\frac{1}{300} eV$ , and  $k_B T$  is expected to be roughly  $\frac{1}{40} eV$ . This means that  $\frac{U_{DH}}{k_B T}$  is expected to be fairly close to 0, so the approximation  $\frac{S_p}{1 - S_p} \approx S_p$  of Equation (7) can still be reasonably made. Therefore, Equation (7) can be modified to develop an expression for the proportion of structured water in PAW, as shown in Equation (8):

$$S_p = 8.1 \times 10^{-5} \exp \left[ \frac{3.6 \text{ kcal/mol} - P \times 9.98 \text{ cm}^3/\text{mol} + U_{DH}}{k_B T} \right] \quad (8)$$

A viscosity model can also be made for PAW, where  $\eta_p = \eta_0 T^{3/2} \exp [E_{ap} / (k_B T)]$  and  $E_{ap} = E_a^B + \Delta E_a S_p$ .

Now,  $\Delta S = S_p - S$  and  $\Delta \eta = \eta_p - \eta$  can be calculated to find the changes in  $S$  and  $\eta$  in PAW compared to distilled water, as shown in Equations (9) and (10), respectively:

$$\begin{aligned} \Delta S &= S_p - S = \frac{g_s}{g_a} \exp \left[ \frac{\Delta u - P\Delta v + U_{DH}}{k_B T} \right] - \frac{g_s}{g_a} \exp \left[ \frac{\Delta u - P\Delta v}{k_B T} \right] \\ &= \frac{g_s}{g_a} \exp \left[ \frac{\Delta u - P\Delta v}{k_B T} \right] \times \left( \exp \left[ \frac{U_{DH}}{k_B T} \right] - 1 \right) \end{aligned}$$

And now, with Equation (3),  $S = \frac{g_s}{g_a} \exp \left[ \frac{\Delta u - P\Delta v}{k_B T} \right]$ ,  $\Delta S$  changes to

$$\Delta S = S \times \left( \exp \left[ \frac{U_{DH}}{k_B T} \right] - 1 \right) \quad (9)$$

$$\Delta \eta = \eta_p - \eta = \eta_0 T^{3/2} \exp [E_{ap} / (k_B T)] - \eta_0 T^{3/2} \exp [E_a / (k_B T)]$$

$$\begin{aligned}
 &= \eta_0 T^{\frac{3}{2}} \left( \left( \exp \left[ \frac{E_a^B}{k_B T} \right] \times \exp \left[ \frac{\Delta E_a S_p}{k_B T} \right] \right) - \left( \exp \left[ \frac{E_a^B}{k_B T} \right] \times \exp \left[ \frac{\Delta E_a S}{k_B T} \right] \right) \right) \\
 &= \eta_0 T^{\frac{3}{2}} \exp \left[ \frac{E_a^B}{k_B T} \right] \times \exp \left[ \frac{\Delta E_a S}{k_B T} \right] \times \left( \exp \left[ \frac{\Delta E_a \Delta S}{k_B T} \right] - 1 \right)
 \end{aligned}$$

Since  $\eta = \eta_0 T^{\frac{3}{2}} \exp[E_a / (k_B T)]$ ,  $\Delta\eta$  changes to

$$\Delta\eta = \eta \times \left( \exp \left[ \frac{\Delta E_a \Delta S}{k_B T} \right] - 1 \right) \tag{10}$$

Under typical conditions,  $\frac{\Delta E_a \Delta S}{k_B T}$  is expected to be less than 1, so the following approximation can be made:  $\exp \left[ \frac{\Delta E_a \Delta S}{k_B T} \right] - 1 \approx \frac{\Delta E_a \Delta S}{k_B T}$ . Therefore, Equation (10) becomes

$$\Delta\eta = \eta \times \frac{\Delta E_a \Delta S}{k_B T} \tag{11}$$

Also, since  $\Delta S = S \times \left( \exp \left[ \frac{U_{DH}}{k_B T} \right] - 1 \right)$  and  $\frac{U_{DH}}{k_B T} \approx \frac{1/300eV}{1/40eV} < 1$ , the same approximation can be made:  $\exp \left[ \frac{U_{DH}}{k_B T} \right] - 1 \approx \frac{U_{DH}}{k_B T}$ . Thus, Equation (9) can be changed to

$$\Delta S = S \times \frac{U_{DH}}{k_B T} \tag{12}$$

The remaining unknown parameter in the formula for  $\Delta\eta$  is  $\Delta E_a$ . This value can be found by fitting the formula to the experimental data. M Shaji et al. [26] found that at 10 °C, PAW at a pH of 2.78 has a kinematic viscosity of 1.28 mm<sup>2</sup>/s. Dynamic viscosity can be found by multiplying the kinematic viscosity of a sample by its density. The density of a PAW sample of a similar pH was measured by weighing the sample and dividing this mass by the volume of the sample upon cooling to 10 °C in a laboratory chiller. The PAW sample was prepared using the same procedure as the original sample used for the experiments conducted by M Shaji et al. [26]; PAW was produced using gliding arc plasma (GAP), a transitional plasma. GAP was produced by creating a vortex between two electrodes by supplying air tangentially between them, and energy was then supplied to produce plasma. The power supplied to produce this sample was 700 W, and the parameters of this sample were pH—2.78; nitrate concentration—100 mg/L; and peroxide concentration—25 mg/L. The PAW was then filtered using a sieve with a mesh size of 63 microns. Measurements of density were performed after the filtration. The density was found to be 0.995 g/mL. Therefore, the dynamic viscosity of PAW at 10 °C was 1.28 mPas. From literature, the dynamic viscosity of distilled water at 10 °C is 1.31 mPas [35]. This means that  $\eta = 1.31 \text{ mPas}$ , and  $\Delta\eta = 1.28 \text{ mPas} - 1.31 \text{ mPas} = -0.03 \text{ mPas}$ . At 10 °C and a pressure of 1 atm,  $S = 0.0455$ , and  $\Delta S = S \times \frac{U_{DH}}{k_B T} \approx S \times \frac{1/300eV}{1/40eV} = 0.00607$ . Therefore, from Equation (11),  $\Delta E_a = \frac{\Delta\eta}{\eta} \times \frac{k_B T}{\Delta S} = -0.12eV$ , and

$$\Delta\eta = \eta \times \left( \exp \left[ -0.12eV \times S \times U_{DH} / (k_B T)^2 \right] - 1 \right) \tag{13}$$

Rearranging (13) yields

$$\frac{\Delta\eta}{\eta} = \left( \exp \left[ -0.12eV \times S \times U_{DH} / (k_B T)^2 \right] - 1 \right) \approx \frac{-0.12eV \times S \times U_{DH}}{(k_B T)^2}$$

Here, we can see that if all variables except for  $T$  are held constant, as  $T$  changes,  $\frac{\Delta\eta}{\eta}$  should follow a curve proportional to  $\frac{1}{T^2} \exp \left[ \frac{1}{T} \right]$ .

$$\frac{\Delta\eta}{\eta} \propto \frac{1}{T^2} \exp \left[ \frac{1}{T} \right] \tag{14}$$

### 3. Results and Discussion

As we have seen,  $\frac{\Delta\eta}{\eta}$  should follow a curve proportional to  $\frac{1}{T^2} \exp\left[\frac{1}{T}\right]$ . From the values already calculated above for PAW with pH 2.7 at 10 °C, we can calculate  $\frac{\Delta\eta}{\eta}$  as follows:

$$\frac{\Delta\eta}{\eta} = \frac{-0.03 \text{ mPas}}{1.31 \text{ mPas}} = -0.02$$

Similarly, the dynamic viscosity of PAW with pH 2.7 was found by measurements of 1.41 and 1.34 mPas at 5 and 8 °C, respectively. Using the viscosity values of distilled water at 5 and 8 °C reported in reference [35], the  $\frac{\Delta\eta}{\eta}$  values for PAW with pH 2.7 at 5 and 8 °C are  $-0.067$  and  $-0.037$ . In order to represent the accuracy of the viscosity measurement methodology, the viscosity of distilled water was measured at temperatures where the PAW viscosities were studied. The measured values and the values reported in the literature for the viscosity of distilled water are in good agreement; these data are shown in Table 1. The measured viscosity values of PAW are shown in Table 2.

**Table 1.** Dynamic viscosity values of distilled water measured and those reported in the literature.

Temperature °C	Measured Distilled Water Viscosity (mPas)	Measurement Error (mPas)	Distilled Water Viscosity from the Literature (mPas) [35]
5	1.51	0.001	1.51
8	1.37	0.006	1.38
10	1.31	0.005	1.31
20	1.02	0.003	1.00

**Table 2.** Dynamic viscosity values of distilled water and PAW samples of pH 2.7 at 5, 8, and 10 °C.

Temperature °C	PAW pH 2.7 Viscosity (mPas)	Measurement Error (mPas)	Distilled Water Viscosity (mPas) [35]
5	1.41	0.009	1.51
8	1.34	0.008	1.38
10	1.28	0.000	1.31

If the model of viscosity of PAW proposed above, as seen in (14), is accurate, then the points (5 °C,  $-0.067$ ), (8 °C,  $-0.037$ ), and (10 °C,  $-0.02$ ) should be found on a curve of the form  $\frac{\Delta\eta}{\eta} = a \times \frac{1}{T^2} \times \exp\left[\frac{1}{T}\right]$ , where  $a$  is a constant. Plotting these points and this curve and adjusting  $a$  to best match the points result in Figure 2.

As shown in Figure 2, the data points fall quite close to the curve, indicating that the proposed model can effectively predict the viscosity of PAW at varying temperatures. Moreover, the model accurately depicts the behavior of PAW viscosity becoming increasingly lower than that of distilled water as the temperature decreases.

With the same rearranged form of Equation (13), it can also be seen that with all else constant, any change in  $U_{DH}$  should result in a proportional change in  $\frac{\Delta\eta}{\eta}$ . If we consider only the contribution of  $H^+$  ions to the  $U_{DH}$  term (let this contribution of  $H^+$  to  $U_{DH}$  be named  $U_{DHH+}$ ),  $U_{DHH+}$  is roughly proportional to  $N_{H+zH+}^2$ , as seen in Equation (5). The charge of  $H^+$  ions is  $+1$ , so  $N_{H+zH+}^2 = N_{H+}$ . Although there are more ions in PAW than just  $H^+$  ions, it is a reasonable approximation that  $U_{DH}$  is roughly proportional to  $U_{DHH+}$ , which, in turn, is proportional to  $N_{H+}$ . Therefore,  $\frac{\Delta\eta}{\eta}$  should be approximately proportional to the  $H^+$  concentration, which is equal to  $10^{-pH}$ .

$$\frac{\Delta\eta}{\eta} \propto 10^{-pH} \tag{15}$$

It is important to note that this model is only applicable for temperatures below roughly 15 °C because it is in this range that the primary effect of active species is reducing viscosity by interfering with the hydrogen bonding between water molecules. Above 15 °C, the active species, which are generally larger than water molecules, have the effect of increasing viscosity due to their size and the absence of many hydrogen bonds in the water itself. This phenomenon was demonstrated by measuring the viscosities of PAW with 2.95 pH at 10 °C and 20 °C; the measurements are shown in Figure 3.

From the data shown in Figure 3, it appears that the crossing-over temperature is found around 15 °C. This is quite similar to the crossing-over temperature found by M Shaji et al. [26], and this again proves the unusual PAW effect of decreasing viscosity at low temperatures.

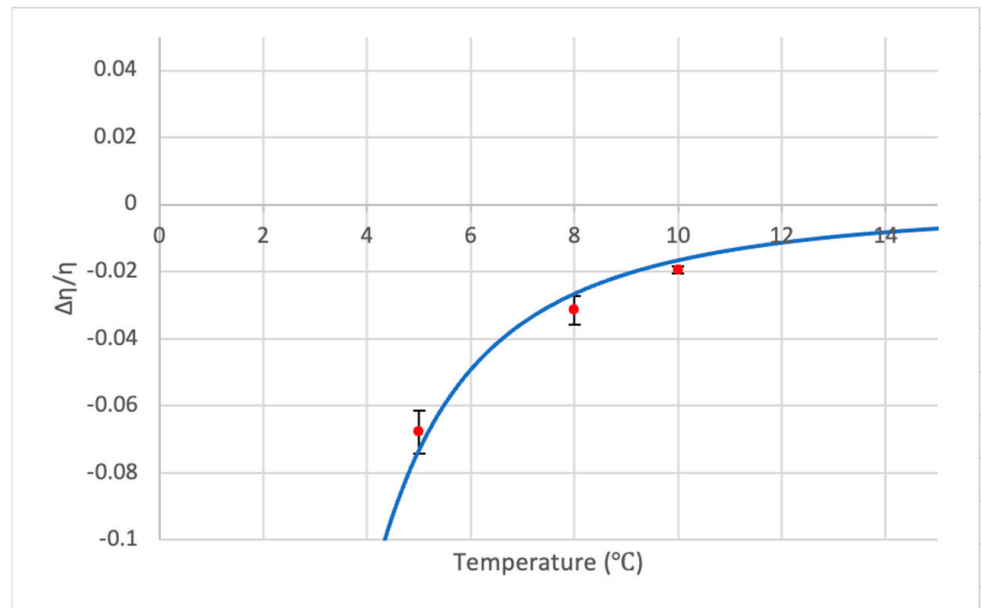


**Figure 2.**  $\frac{\Delta\eta}{\eta}$  (shown in red dots) at temperatures of 5 °C, 8 °C, and 10 °C along with the curve (shown in blue line) of  $\frac{\Delta\eta}{\eta} = \frac{a}{T^2} \times \exp\left[\frac{1}{T}\right]$ , where  $a = -1.5$ .

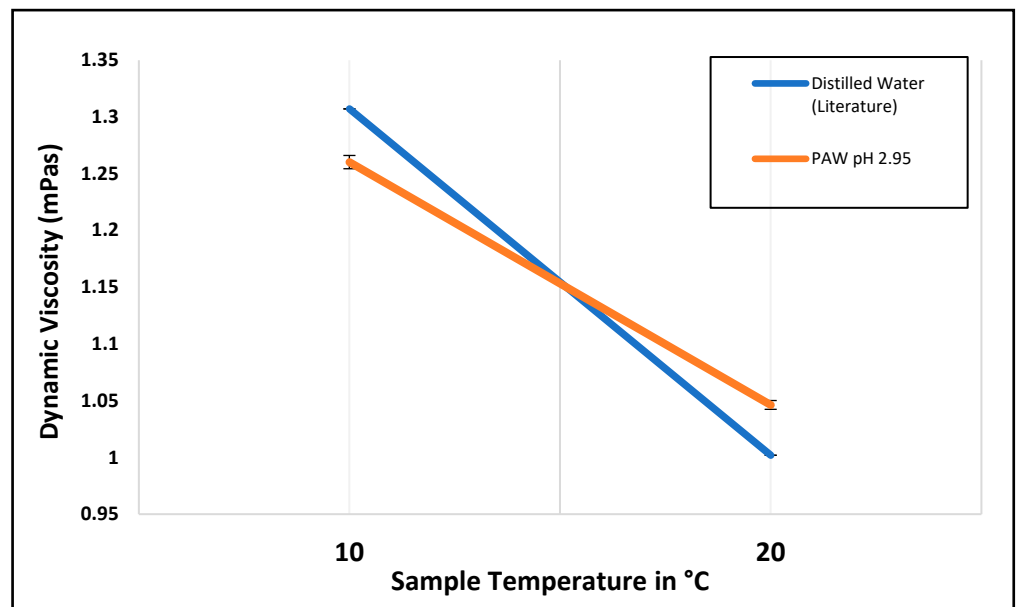


**Figure 3.** The dynamic viscosities of distilled water [35] and PAW at pH 2.95 at 10 °C and 20 °C.

In order to see the difference in the PAW viscosity with respect to varied pH values, PAW with a pH ranging from 2.95 to 3.45 was produced using gliding arc plasma. The PAW was prepared using the same production and filtration procedures as described before. This time, the power supplied was between 350 and 400 W, the nitrate concentration was 250 mg/L, and the peroxide concentration was 150 mg/L. The pH was measured using a Hanna growline monitor with an accuracy of within 0.05 pH. The procedure for measuring the viscosity was also the same as that used by M Shaji et al. [26]; the kinematic viscosity was measured using a size 25 cannon-Fenske viscometer, the certified accuracy of which is 0.16%. A laboratory chiller was used to keep the temperature of the PAW samples constant at 10 °C during the density and viscosity measurements. The kinematic viscosity values were then multiplied by the density of the sample to obtain the dynamic viscosity. The dynamic viscosities of different PAW samples are shown in the Table 3 below; the dynamic viscosity of distilled water from the literature is included for comparison [35].

**Table 3.** Dynamic viscosity values of distilled water and PAW samples at 10 °C.

Sample	Dynamic Viscosity (mPas)	Measurement Error (mPas)
Distilled Water	1.31 [35]	-
PAW, pH 2.95	1.26	0.005
PAW, pH 3.04	1.27	0.003
PAW, pH 3.45	1.29	0.005

Now, by using the data in Table 3, we can determine if  $\frac{\Delta\eta}{\eta}$  is proportional to  $10^{-pH}$ . Using the dynamic viscosity values at 10 °C, for each PAW sample, we calculate  $\frac{\Delta\eta}{\eta} = \frac{\eta_p - \eta}{\eta}$ , where  $\eta_p$  is the dynamic viscosity of the given PAW sample, and  $\eta$  is the dynamic viscosity of distilled water. Plotting these values against the pH of each sample gives Figure 4.

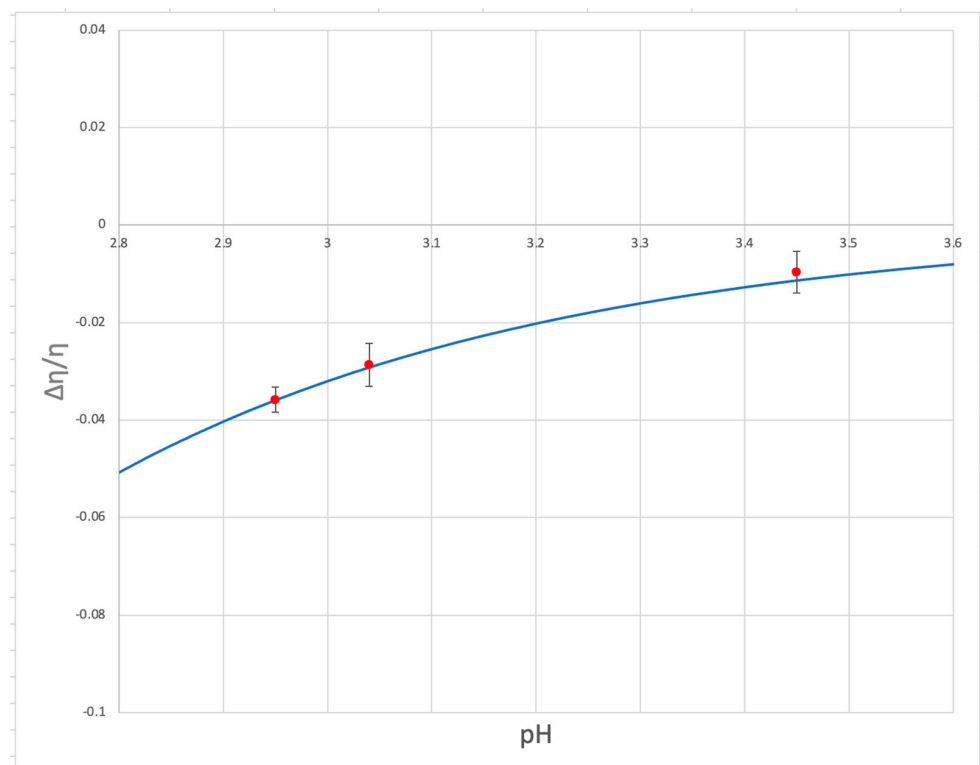


**Figure 4.**  $\frac{\Delta\eta}{\eta}$  (shown in red dots) calculated for PAW at pH 2.95, 3.04, and 3.45 along with the curve (shown in blue line) of  $\frac{\Delta\eta}{\eta} = c \times 10^{-pH}$ , where  $c = -32$ .

The data in Figure 4 fall nearly perfectly on the theoretical curve, again indicating that the model, as seen in (15), proposed for the viscosity of PAW is quite accurate, particularly at lower temperatures. Given that the viscosity model is an accurate predictor of the experimental viscosity data, it can be concluded that the general model for the proportion of nano-crystalline structures in PAW is also a useful and accurate means to understand the structure and behavior of PAW.

#### 4. Conclusions

- This study constructed a model that explains the following:
  - How PAW induces the significant effects observed on physical properties, such as washing-out ability, surface tension, contact angle, and viscosity;
  - Why PAW has the surprising effect of lowering the viscosity at lower temperatures;
  - How the effects of PAW exceed the colligative effect for ideal solutions.
- A model for the proportion of nano-crystalline structures in PAW and a model for PAW viscosity were developed using the two-state model of water and the Debye–Huckel theory, along with the assumption that the effects of plasma-generated species are small enough to be approximated as linear.
- This viscosity model predicts the following:
  - Below 15 °C,  $\frac{\Delta\eta}{\eta}$  is proportional to  $\frac{1}{T^2} \times \exp\left[\frac{1}{T}\right]$  and  $10^{-pH}$ .
  - As the temperature decreases, the viscosity of PAW becomes increasingly lower than the viscosity of distilled water, thus explaining PAW’s unusual viscosity-reducing effect; furthermore, although the contribution of the Debye–Huckel term was approximated to be linear, the full form of the model contains two exponential terms, one inside the other, which can explain why the effect of PAW is non-colligative
- Even with the approximations, the viscosity model proved to match the experimental data quite well, demonstrating a strong ability of the equation to accurately predict the PAW viscosity.
- The proportion of nano-crystalline structures in water and PAW determines many physical properties beyond the viscosity, so the model of PAW developed here could be used to understand and model any of these physical properties, potentially facilitating many applications of PAW, such as the use as an eco-friendly surfactant or disinfectant of fresh produce. While the present work has not yet modeled physical properties outside of the viscosity, the success of the viscosity model alone shows promise for the modeling of other properties.

**Author Contributions:** Conceptualization, A.F. and A.R.; methodology, A.F., A.R. and J.G.; software, J.G. and D.V.; validation, M.S. and J.G.; formal analysis, J.G. and M.S.; investigation, J.G. and M.S.; resources, A.F. and A.R.; data curation, J.G.; writing—original draft preparation, J.G.; writing—review and editing, J.G., A.F., A.R. and M.S.; visualization, J.G.; supervision, A.R., A.F. and C.S.; project administration, A.F. and A.R. All authors have read and agreed to the published version of the manuscript.

**Funding:** This research received no external funding.

**Institutional Review Board Statement:** Not applicable.

**Data Availability Statement:** The data that support the findings of this study are available from the corresponding author, M.S., upon request.

**Conflicts of Interest:** The authors declare no conflict of interest.

#### References

1. Fridman, A. *Plasma Chemistry*; Cambridge University Press: Cambridge, UK, 2008.
2. Zhou, R.; Zhou, R.; Wang, P.; Xian, Y.; Mai-Prochnow, A.; Lu, X.; Cullen, P.J.; Ostrikov, K.K.; Bazaka, K. Plasma-Activated Water: Generation, Origin of Reactive Species and Biological Applications. *J. Phys. Appl. Phys.* **2020**, *53*, 303001. [[CrossRef](#)]

3. Fridman, A.A. *Plasma Medicine*; John Wiley & Sons: Chichester, UK, 2013; ISBN 978-1-118-43765-0.
4. Cooper, M.; Fridman, G.; Staack, D.; Gutsol, A.F.; Vasilets, V.N.; Anandan, S.; Cho, Y.I.; Fridman, A.; Tsapin, A. Decontamination of Surfaces from Extremophile Organisms Using Nonthermal Atmospheric-Pressure Plasmas. *IEEE Trans. Plasma Sci.* **2009**, *37*, 866–871. [[CrossRef](#)]
5. Nunnally, T.; Gutsol, K.; Rabinovich, A.; Fridman, A.; Starikovskiy, A.; Gutsol, A.; Potter, R.W. Dissociation of H<sub>2</sub>S in Non-Equilibrium Gliding Arc “Tornado” Discharge. *Int. J. Hydrogen Energy* **2009**, *34*, 7618–7625. [[CrossRef](#)]
6. Stratton, G.R.; Bellona, C.L.; Dai, F.; Holsen, T.M.; Thagard, S.M. Plasma-Based Water Treatment: Conception and Application of a New General Principle for Reactor Design. *Chem. Eng. J.* **2015**, *273*, 543–550. [[CrossRef](#)]
7. Palma, D.; Papagiannaki, D.; Lai, M.; Binetti, R.; Sleiman, M.; Minella, M.; Richard, C. PFAS Degradation in Ultrapure and Groundwater Using Non-Thermal Plasma. *Molecules* **2021**, *26*, 924. [[CrossRef](#)] [[PubMed](#)]
8. Lewis, A.J.; Joyce, T.; Hadaya, M.; Ebrahimi, F.; Dragiev, I.; Giardetti, N.; Yang, J.; Fridman, G.; Rabinovich, A.; Fridman, A.A.; et al. Rapid Degradation of PFAS in Aqueous Solutions by Reverse Vortex Flow Gliding Arc Plasma. *Environ. Sci. Water Res. Technol.* **2020**, *6*, 1044–1057. [[CrossRef](#)]
9. Surace, M.J.; Murillo-Gelvez, J.; Shaji, M.A.; Fridman, A.A.; Rabinovich, A.; McKenzie, E.R.; Fridman, G.; Sales, C.M. Plasma-Assisted Abatement of Per- and Polyfluoroalkyl Substances (PFAS): Thermodynamic Analysis and Validation in Gliding Arc Discharge. *Plasma* **2023**, *6*, 419–434. [[CrossRef](#)]
10. Foster, J.E. Plasma-Based Water Purification: Challenges and Prospects for the Future. *Phys. Plasmas* **2017**, *24*, 055501. [[CrossRef](#)]
11. Saleem, M.; Tomei, G.; Beria, M.; Marotta, E.; Paradisi, C. Highly Efficient Degradation of PFAS and Other Surfactants in Water with Atmospheric RADial Plasma (RAP) Discharge. *Chemosphere* **2022**, *307*, 135800. [[CrossRef](#)]
12. Khan, M.J.; Jovicic, V.; Zbogar-Rasic, A.; Poser, A.; Freichels, K.; Delgado, A. Effectiveness of Non-Thermal Plasma Induced Degradation of Per- and Polyfluoroalkyl Substances from Water. *Water* **2022**, *14*, 1408. [[CrossRef](#)]
13. Johnson, M.J.; Maza, W.A.; Breslin, V.M.; Boris, D.R.; Petrova, T.B.; Walton, S.G. Low Power Degradation of Perfluorooctane Sulfonate (PFOS) in Water Using a Nanosecond Pulsed Atmospheric Pressure Plasma. *Plasma Sources Sci. Technol.* **2022**, *31*, 085001. [[CrossRef](#)]
14. Foster, J.E.; Mujovic, S.; Groele, J.; Blankson, I.M. Towards High Throughput Plasma Based Water Purifiers: Design Considerations and the Pathway towards Practical Application. *J. Phys. Appl. Phys.* **2018**, *51*, 293001. [[CrossRef](#)]
15. Moszczyńska, J.; Liu, X.; Wiśniewski, M. Non-Thermal Ammonia Decomposition for Hydrogen Production over Carbon Films under Low-Temperature Plasma—In-Situ FTIR Studies. *Int. J. Mol. Sci.* **2022**, *23*, 9638. [[CrossRef](#)] [[PubMed](#)]
16. Li, W.; Cao, M.; Meng, S.; Li, Z.; Xu, H.; Liu, L.; Song, H. Non-Thermal Plasma Assisted Catalytic Water Splitting for Clean Hydrogen Production at near Ambient Conditions. *J. Clean. Prod.* **2023**, *387*, 135913. [[CrossRef](#)]
17. Mumtaz, S.; Khan, R.; Rana, J.N.; Javed, R.; Iqbal, M.; Choi, E.H.; Han, I. Review on the Biomedical and Environmental Applications of Nonthermal Plasma. *Catalysts* **2023**, *13*, 685. [[CrossRef](#)]
18. Gapper, C.; Dolan, L. Control of Plant Development by Reactive Oxygen Species. *Plant Physiol.* **2006**, *141*, 341–345. [[CrossRef](#)]
19. Judée, F.; Simon, S.; Bailly, C.; Dufour, T. Plasma-Activation of Tap Water Using DBD for Agronomy Applications: Identification and Quantification of Long Lifetime Chemical Species and Production/Consumption Mechanisms. *Water Res.* **2018**, *133*, 47–59. [[CrossRef](#)]
20. Ma, R.; Wang, G.; Tian, Y.; Wang, K.; Zhang, J.; Fang, J. Non-Thermal Plasma-Activated Water Inactivation of Food-Borne Pathogen on Fresh Produce. *J. Hazard. Mater.* **2015**, *300*, 643–651. [[CrossRef](#)]
21. Guo, L.; Yao, Z.; Yang, L.; Zhang, H.; Qi, Y.; Gou, L.; Xi, W.; Liu, D.; Zhang, L.; Cheng, Y.; et al. Plasma-Activated Water: An Alternative Disinfectant for S Protein Inactivation to Prevent SARS-CoV-2 Infection. *Chem. Eng. J.* **2021**, *421*, 127742. [[CrossRef](#)]
22. Li, Y.; Pan, J.; Ye, G.; Zhang, Q.; Wang, J.; Zhang, J.; Fang, J. In Vitro Studies of the Antimicrobial Effect of Non-Thermal Plasma-Activated Water as a Novel Mouthwash. *Eur. J. Oral Sci.* **2017**, *125*, 463–470. [[CrossRef](#)]
23. Ten Bosch, L.; Köhler, R.; Ortmann, R.; Wieneke, S.; Viöl, W. Insecticidal Effects of Plasma Treated Water. *Int. J. Environ. Res. Public Health* **2017**, *14*, 1460. [[CrossRef](#)] [[PubMed](#)]
24. Rathore, V.; Nema, S.K. The Role of Different Plasma Forming Gases on Chemical Species Formed in Plasma Activated Water (PAW) and Their Effect on Its Properties. *Phys. Scr.* **2022**, *97*, 065003. [[CrossRef](#)]
25. He, J.; Rabinovich, A.; Vainchtein, D.; Fridman, A.; Sales, C.; Shneider, M.N. Effects of Plasma on Physical Properties of Water: Nanocrystalline-to-Amorphous Phase Transition and Improving Produce Washing. *Plasma* **2022**, *5*, 462–469. [[CrossRef](#)]
26. Shaji, M.; Rabinovich, A.; Surace, M.; Sales, C.; Fridman, A. Physical Properties of Plasma-Activated Water. *Plasma* **2023**, *6*, 45–57. [[CrossRef](#)]
27. Brini, E.; Fennell, C.J.; Fernandez-Serra, M.; Hribar-Lee, B.; Lukšič, M.; Dill, K.A. How Water’s Properties Are Encoded in Its Molecular Structure and Energies. *Chem. Rev.* **2017**, *117*, 12385–12414. [[CrossRef](#)] [[PubMed](#)]
28. Semak, V.V.; Gerakis, A.; Shneider, M.N. Measurement of Temperature Dependent Absorption Coefficient of Water at 1064 nm Wavelength. *AIP Adv.* **2019**, *9*, 085016. [[CrossRef](#)]
29. Boles, M.A.; Dr, Y.A.C. *Thermodynamics: An Engineering Approach*; McGraw-Hill Education: New York, NY, USA, 2014; ISBN 978-0-07-339817-4.
30. Tanaka, H. Simple Physical Model of Liquid Water. *J. Chem. Phys.* **2000**, *112*, 799–809. [[CrossRef](#)]
31. Fisher, M.E. The Theory of Equilibrium Critical Phenomena. *Rep. Prog. Phys.* **1967**, *30*, 615. [[CrossRef](#)]

32. Olmsted, P.D. Lectures on Landau Theory of Phase Transitions. Available online: [https://site.physics.georgetown.edu/~pdo7/ps\\_files/landau.pdf](https://site.physics.georgetown.edu/~pdo7/ps_files/landau.pdf) (accessed on 1 July 2023).
33. Redfern, S. Order-Disorder Phase Transitions. *Rev. Mineral. Geochem.* **2000**, *39*, 105–133. [[CrossRef](#)]
34. Shen, Y.; Wei, X.; Wang, Y.; Shen, Y.; Li, L.; Huang, Y.; Ostrikov, K. Energy Absorbancy and Freezing-Temperature Tunability of NaCl Solutions during Ice Formation. *J. Mol. Liq.* **2021**, *344*, 117928. [[CrossRef](#)]
35. Kestin, J.; Sokolov, M.; Wakeham, W.A. Viscosity of Liquid Water in the Range  $-8\text{ }^{\circ}\text{C}$  to  $150\text{ }^{\circ}\text{C}$ . *J. Phys. Chem. Ref. Data* **1978**, *7*, 941–948. [[CrossRef](#)]

**Disclaimer/Publisher’s Note:** The statements, opinions and data contained in all publications are solely those of the individual author(s) and contributor(s) and not of MDPI and/or the editor(s). MDPI and/or the editor(s) disclaim responsibility for any injury to people or property resulting from any ideas, methods, instructions or products referred to in the content.